Three-Dimensional Local Structure of Photoexcited Cu Diimine Complex Refined by Quantitative XANES Analysis

Grigory Smolentsev,*,† Alexander V. Soldatov,† and Lin X. Chen‡,§

Faculty of Physics, Southern Federal University, Sorge 5, Rostov-on-Don 344090, Russia, Chemical Sciences and Engineering Division, Argonne National Laboratory, 9700 South Cass Avenue, Argonne, Illinois 60439, and Department of Chemistry, Northwestern University, 2145 Sheridan Road, Evanston, Illinois 60208

Received: February 17, 2008

The structural details of $[Cu(dmp)_2]^+$ (dmp = 2,9-dimethyl-1,10-phenanthroline) at its metal-to-ligand charge-transfer (MLCT) excited-state in acetonitrile were extracted using quantitative analysis of Cu K-edge X-ray adsorption near edge structure (XANES). The study combines two techniques: fitting experimental XANES spectra with a multidimensional interpolation approximation, and calculating theoretical XANES spectra with molecular potentials beyond the muffin-tin approximation. The results of the study show that the best fit of the experimental XANES data must include a solvent molecule binding to the Cu with a short Cu−N distance of 2.00 Å. This confirms that the formation of an exciplex is responsible for the excited-state quenching in coordinating solvents, such as acetonitrile. Moreover, the calculations suggest that the formation of this exciplex state is accompanied by significant rocking distortions of the dmp ligands resulting in a 108° angle between the N(solvent)−Cu bond and the C_2 symmetry axis of the dmp ligand. This combined approach allows us to extract molecular configurations that would otherwise be missed in a conventional qualitative XANES analysis.

1. Introduction

Photoinduced charge-transfer processes have been among the most studied chemical reactions because of their relevance to molecular devices, photocatalysis, and solar energy conversion/storage.[1–8] Understanding the molecular structures and dynamics of both photoexcited states and charge-separated intermediates is crucial not only for their broad applications, but also for their fundamental importance in gaining insight into the nature of photochemical reactions. It enables one to develop theoretical models for predicting the reaction mechanisms and dynamics for photoinduced processes.

Recently laser-initiated time-resolved X-ray absorption spectroscopy (LITR-XAS) has opened new possibilities for investigating local structures of photoexcited molecules.[9–12] This technique, also known as pump-and-probe X-ray absorption spectroscopy or X-ray transient absorption (XTA), consists of a UV−vis pump laser pulse that triggers a photoinduced process, and a hard X-ray probe−pulse that interrogates structural changes induced by the pump. Typically, the time resolution of such experiments at a synchrotron facility is around 100 ps and is limited mainly by the single electron bunch duration. Although the bunch slicing technique could achieve X-ray pulses with 100 fs duration,[13,14] a 1000-fold reduction in the photon flux in an X-ray bunch limits its applications to a very small number of samples. Forthcoming X-ray free electron lasers will eradicate this obstacle because of its high pulse photon flux and short pulse duration. However, their spectral tunability is limited in comparison with the synchrotron based X-ray sources for spectroscopy studies.[15–17] For this reason, XTA employed in currently available synchrotron sources is still suitable for investigating excited-state structures with lifetimes longer than a few hundred picoseconds, as demonstrated in the literature.[18–28] XTA's ability to obtain excited-state electronic and geometric structural information makes it a powerful technique for solving local structures around heavy atoms in disordered media, complementing those acquired from the pump−probe X-ray diffraction for single crystals.[29–31]

Although, traditionally, interatomic distances have been extracted by analyses of the extended X-ray absorption fine structure (EXAFS), recently developed algorithms allow quantitative determination of bond lengths and angles from X-ray adsorption near edge structure (XANES) spectra.[32–35] This technique has been recently applied to different metal complexes.[36–42] Moreover, XANES spectra of photoexcited molecules can also be calculated using either time-dependent density functional theory (TD-DFT) or time-dependent Hartree−Fock (TD-HF) theory.[43] The primary advantage of XANES analyses is that it can provide not only the radial distribution of the atoms, as in conventional EXAFS analysis, but also the three-dimensional arrangements of the atoms.

Here we conduct an XANES analysis using the above-mentioned approach[32] for a metal-to-ligand charge-transfer (MLCT) excited-state structure of a copper(I) diimine complex, $[Cu(dmp)_2]^+$ (dmp = 2,9-dimethyl-1,10-phenanthroline) in acetonitrile. According to the ultrafast optical transient absorption data, the excited-state kinetics of $[Cu(dmp)_2]^+$ can be characterized by a triexponential function with time constants of 500−700 fs, 10−20 ps, and 1.6−1.7 ns.[20,44] The currently accepted mechanism of photochemical transformations includes the following steps: (1) excitation to the Franck−Condon state with a pseudo-tetrahedral coordination geometry of Cu as in the ground state, (2) Jahn−Teller distortions of the transient Cu(II) with $3d^9$ electronic configuration to a "flattened" tetrahedral coordination geometry characterized by the decrease of the dihedral angle between two dmp ligand planes, and (3) the formation of an exciplex between the MLCT excited-state and a strong Lewis basic solvent molecule, resulting in the

* Corresponding author. E-mail: smolentsev@yandex.ru.
† Southern Federal University.
‡ Argonne National Laboratory.
§ Northwestern University.

10.1021/jp801410a CCC: $40.75
Published on Web 05/28/2008

excited-state quenching. Although distances between Cu and other nearest-neighboring atoms have been obtained from previous studies,[19,20] the exact geometry of the final thermally equilibrated MLCT state, or the exciplex state, is not completely known. Quantum chemistry calculations, based on the DFT implemented in Gaussian[45] and ADF[46] codes, have predicted significant flattening distortions (up to 35°) with very small rocking distortions (less than 5°).[20,47,48] These theoretical results were supported by the crystal structure of [Cu(II)(dpp)$_2$]$^{2+}$ (dpp = 2,9-diphenyl-1,10-phenanthroline), thereby mimicking the Cu(II) at the MLCT state, even though [Cu(II)(dpp)$_2$]$^{2+}$ has phenyl groups shielding Cu(II) from solvent molecules.[49] The Cu(II)−N_{CH3CN} distance was 3.05 Å obtained from the ADF calculations for the exciplex.[20] However, even for the ground-state complex, Cu−N_{dmp} bond length varies within 0.05 Å range depending on the basis set and the code used in the calculations.[47,48,50] The latest DFT calculations for the exciplex[20] yielded an average Cu−N_{dmp} distance of 2.0 Å. This model is somewhat contradictory with the X-ray diffraction data for a related Cu(II) phenanthroline complex cocrystallized with acetonitrile.[51] The structure of this acetonitrle complex has a Cu−N_{CH3CN} bond length of 2.05 Å, and a significant rocking distortion. This distortion was characterized by an angle of 113° between the N_{CH3CN}−Cu bond and the C_2 axis of the dmp ligand. The pump−probe EXAFS data and qualitative analysis of the XANES region suggested the presence of one or possibly two solvent molecules coordinating with Cu.[20] Nevertheless, it was very difficult to separate contributions of Cu−N_{dmp} from that of Cu−N_{CH3CN} in the EXAFS analysis, because of their similarity and the small average Cu−N distance change of 0.04 Å in the MLCT state from that of the ground state. Consequently, there can be at least three models for the exciplex state of [Cu(dmp)$_2$]$^+$ shown in Figure 1: a five-coordinated complex with significant flattening, a six-coordinated complex, and a five-coordinated complex with significant rocking distortions.

The purpose of the present paper is selection of a realistic structural model for the MLCT state of photoexcited [Cu(dmp)$_2$]$^+$ and refinement of bond lengths and angles on the basis of fitting the theoretical calculated spectra with the experimental pump−probe XANES data.

2. Methods

The method of structure determination is based on a combination of quantitative XANES fitting using the multidimensional interpolation approach[32] and full-potential calculations of XANES on the basis of the finite difference method (FDM).[52] Within this approach, the number of required time-consuming FDM calculations of XANES spectra corresponding to different structural models is minimized using the following expansion of the spectrum as a function of the structural parameters:

$$\mu_i(E, p_1 + \delta p_1, p_2 + \delta p_2, ..., p_n + \delta p_n) = \mu(E, p_1, p_2, ..., p_n) + \sum_n A_n(E)\delta p_n + \sum_{m,n} B_{mn}(E)\delta p_m \delta p_n + ... \quad (1)$$

Where $\mu_i(E)$ is the interpolated X-ray absorption coefficient, whereas $\mu(E)$ is the absorption coefficient calculated via FDM, (p_1,p_2, ..., p_n) is a starting set of structural parameters, and δp_n is the deviation of p_n from the starting value. The energy-dependent coefficients, $A_n(E)$, $B_{mn}(E)$, ..., are deduced from the results of FDM calculations. A general description of the multidimensional interpolation and the FDM can be found in refs 32 and 52, respectively. The interpolation nodes (sets of structural parameters used for the energy dependent coefficients $A_n(E)$, $B_{mn}(E)$, ... calculation) are chosen within selected limits of variations, so that the influence of corresponding terms of the expansion and the distance between nodes in the parameter space are maximized, which avoids numerical instabilities that may occur using the method.

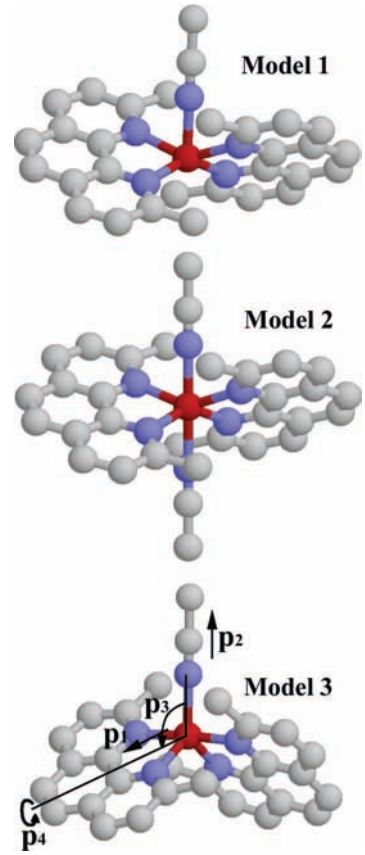

Figure 1. Possible structural models of photoexcited [Cu(dmp)$_2$]$^+$. Top: five-coordinated complex with flattening distortions; middle: six-coordinated complex with flattening distortions; and bottom: five-coordinated complex with rocking distortions. The structural parameters varied in calculations are shown for the bottom complex. N atoms are blue, C atoms are gray, and the Cu atom is red.

The finite difference calculations of Cu K-edge XANES spectra of [Cu(dmp)$_2$]$^+$ were performed for a cluster of 5.0 Å radius surrounding the metal atom. This cluster size was chosen because the calculations of the spectrum as a function of the cluster size confirmed the spectral invariance in larger clusters. The energy-dependent exchange-correlation potential is obtained from the Hedin−Lundqvist approach. For comparison, full multiple scattering calculations with the muffin-tin potential approximation were also performed using the FEFF8.4 code.[53]

Experimental Cu K-edge XTA spectra for the MLCT excited-state [Cu(dmp)$_2$]$^+$ were obtained at Beamline 11ID-D of the Advances Photon Source, and the experimental details can be found elsewhere.[20] Briefly, a second harmonic of a Nd/YLF laser (λ = 527 nm, 1 kHz repetition rate, 1 mJ/pulse, and 5 ps fwhm) was used for the photoexcitation. A time resolution of ~100 ps was achieved using X-ray probe−pulses generated from single electron bunches in the storage ring. The concentration of [Cu(dmp)$_2$]$^+$ in acetonitrile solution was ~2 mM.

3. Results and Discussion

The local structure refinement by our method[32] is based on the general hypothesis that the XANES calculations should

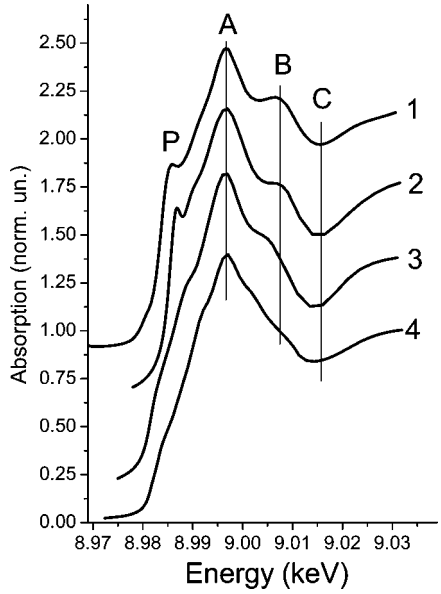

Figure 2. Cu K-edge XANES spectra of $[Cu(dmp)_2]^+$ in the ground-state: experimental (curve 1) and theoretical (curves 2−4). Calculations were performed using the full-potential FDM (FDMNES code) (curve 2), FDM with muffin-tin potential (FDMNES code) (curve 3), and full multiple scattering theory (FEFF8 code) (curve 4).

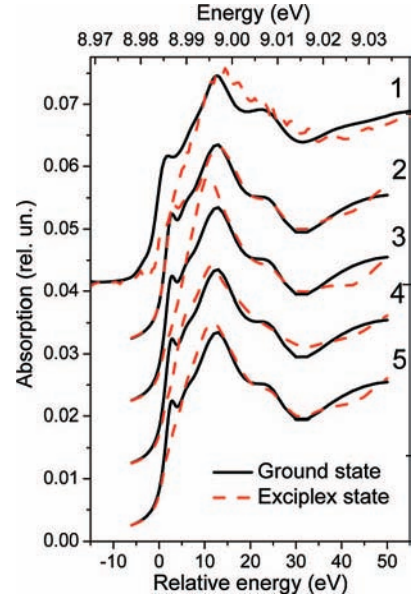

Figure 3. Cu K-edge XANES spectra of $[Cu(dmp)_2]^+$ for the ground-state geometry (black solid lines) and different models of the photo-excited local structures (red dashed lines): experimental (curve 1) and theoretical (curves 2−5). Dashed curve 2 corresponds to model 1 with a long $Cu-N_{CH3CN}$ distance; dashed curve 3 corresponds to model 2 with a short $Cu-N_{CH3CN}$ distance; dashed curve 4 corresponds to model 3 with a short $Cu-N_{CH3CN}$ distance; and dashed curve 5 corresponds to model 1 with a short $Cu-N_{CH3CN}$ distance.

reproduce fine features observed in an experimental spectrum if a correct local structural model is used. This hypothesis has been verified for different systems and more importantly for the ground-state $[Cu(dmp)_2]^+$ with a known local geometry determined by X-ray diffraction.[54] Three different approaches were used in our study: (1) full multiple scattering theory with muffin-tin potential implemented into FEFF8,[53] (2) full-potential FDM, and (3) FDM with muffin-tin potential implemented into FDMNES code.[52]

As one can see from Figure 2, the nonmuffin-tin FDM approach gives the best agreement with the experimental spectrum in all fine features and their relative intensities, especially the pronounced sharp feature P. On the other hand, the muffin-tin calculations produce significantly different spectra with only a very weak P shoulder. Feature B is less intense in the spectra with muffin-tin FDM calculations than that with nonmuffin-tin calculations using the same approach and identical nonstructural parameters, including the line-width broadening. Hence, these results demonstrate that the potential deviation from the muffin-tin approximation must be taken into account in order to have correct quantitative refinements of structural parameters based on XANES calculations.

As it was described in the introduction, there are three possible structural models for the MLCT excited state $[Cu(dmp)_2]^+$ (Figure 1). For each model, two variants were considered: proximal solvent−solute complex ($Cu-N_{CH3CN}$ distance is 2.0−2.2 Å) and distal solvent−solute complex ($Cu-N_{CH3CN}$ distance is 3.05 Å). One can see from curve 2 in Figure 3 that the flattening distortion of the two dmp ligands with a distal solvent molecule does not reproduce the experimental spectrum of the MLCT state, which is featured by a reduction of peak P compared to the spectrum of the ground state. A reduction of peak P intensity can only be obtained for the models with a short $Cu-N_{CH3CN}$ bond, as seen from the comparison of curves 2 and 5. Both curves are based on model 1, but only differ in $Cu-N_{CH3CN}$ distances. Calculations for structures with only flattening distortions alone (curves 2, 3, and 5) do not produce the same level of peak B intensity as seen in the experimental

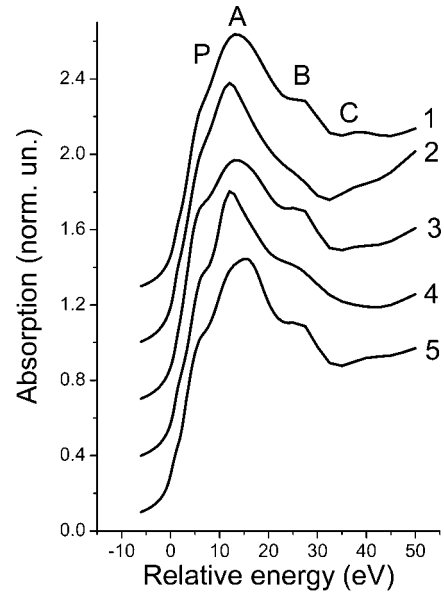

Figure 4. Theoretical Cu K-edge XANES spectra of $[Cu(dmp)_2]^+$ in the photoexcited state calculated for different sets of structural parameters. The trace numbering corresponds to the sets of parameters in Table 1.

spectrum. Only an exciplex state structure with significant rocking distortions of the dmp planes shows such a trend. Thus, we can conclude that model 3 with a short $Cu-N_{CH3CN}$ distance is the most accurate in reproducing the experimental spectra.

The following analysis is focused on the refinement of this model and quantitative determination of the local structure parameters. We have tested sensitivity of calculated XANES spectra to the parameters shown in Figure 1 where p_1 is the average $Cu-N_{dmp}$ distance, p_2 is the $Cu-N_{CH3CN}$ distance, p_3 is the angle between the $Cu-N_{CH3CN}$ bond and the C_2 axis of

TABLE 1: Sets of Structural Parameters That Correspond to the Calculations Presented in Figure 4

set of structural parameters	p_1 ($Cu-N_{dmp}$) (Å)	p_2 ($Cu-N_{CH3CN}$) (Å)	p_3 ($N_{CH3CN}-Cu-C_{2dmp}$) (°)	p_4 (dmp axial rot) (°)
1	1.94	2.0	103	0
2	2.04	2.0	103	0
3	1.94	2.2	103	0
4	1.94	2.0	123	0
5	1.94	2.0	103	20

the dmp ligands, and p_4 is the axial rotation of the dmp groups. In all cases, a C_2 symmetry of the exciplex structure is fixed. Other structural distortions, such as the wagging motions of dmp, which lead to an asymmetric $Cu-N_{dmp}$ bond length change, have insignificant effects on the calculated spectra. Figure 4 shows the effects of geometry variations on shapes of calculated XANES spectra, with corresponding sets of structural parameters summarized in Table 1. Clearly, $Cu-N_{dmp}$ distance and rocking distortions have a significant influence on the intensity of peak B, but these parameters shift the position of valley C in different directions. The elongation of $Cu-N_{CH3CN}$ distance leads to an increase in peak P intensity. Maximum A becomes sharper as a result of either $Cu-N_{dmp}$ distance elongation or an increase of rocking distortions. It shifts to higher energies after axial rotations of dmp ligands. Using the strategy of the polynomial construction described elsewhere[32] for varying the parameters within the limits of p_1 1.94−2.04 Å, p_2 2.0−2.2 Å, p_3 103−123°, and p_4 0−20°, we have obtained the following polynomial to reproduce the FDM calculation results for any set of parameters:

$$\mu_i(E, p_1+\delta p_1, p_2+\delta p_2, p_3+\delta p_3, p_4+\delta p_4) = \mu(E, p_1, p_2, p_3, p_4) + \sum_{i=1}^{4} A_i(E)\delta p_i + \sum_{i=1}^{3}\sum_{\substack{j=3 \\ j\neq i}}^{4} B_{ij}(E)\delta p_i \delta p_j + C_1(E)\delta p_1 \delta p_3 \delta p_4 + C_2(E)\delta p_2 \delta p_3 \delta p_4 \quad (2)$$

Thus only 17 time-consuming FDM calculations are necessary for the XANES fitting (12 spectra correspond to the interpolation nodes, and five spectra were used checking negligibility of some expansion terms).

In our calculations, the discrepancy between the experimental and theoretical results is minimized in the *difference* spectra of the exciplex and the ground states, instead of directly minimizing the discrepancy between theoretical and experimental spectra for each state. This self-referential approach avoids varying structural parameters in order to compensate for the difference between experimental and theoretical spectra due to nonstructural origins, such as those that exist even for the ground state. The following criterion of spectra comparison was used:

$$\min\left(\frac{1}{E_2-E_1}\int_{E_1}^{E_2}[(\mu_{exp}^{es}-\mu_{exp}^{gs})-(\mu_{theor}^{es}-\mu_{theor}^{gs})]^2 dE\right) \quad (3)$$

In this formula μ_{exp}^{es} and μ_{exp}^{gs} are experimental absorption coefficients for the excited and ground states, respectively; μ_{theor}^{es} and μ_{theor}^{gs} are analogous theoretically calculated absorption coefficients, and E_1 and E_2 define the energy range of spectra comparison.

A comparison between the best-fit results with experimental data is presented in Figure 5. We also include the experimental spectrum of $[Cu(II)(dmp)_2]^{2+}$ generated electrochemically, which is almost identical to the spectrum of the exciplex within the experimental error, but has a better signal-to-noise ratio.

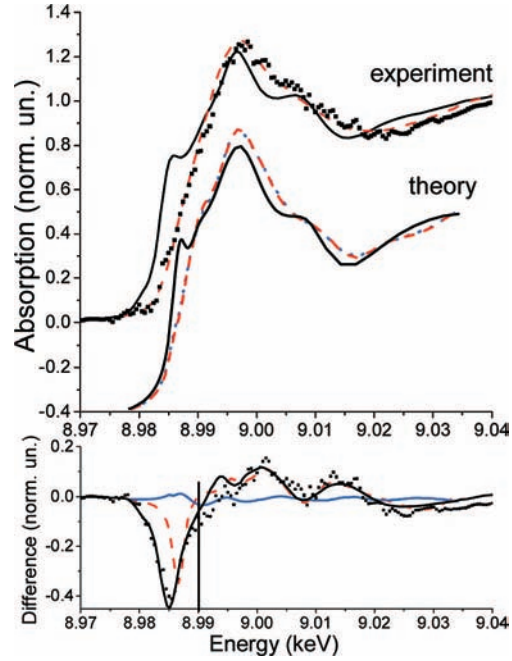

Figure 5. Top panel: Experimental and theoretical Cu K-edge XANES spectra of $[Cu(dmp)_2]^+$. Solid lines correspond to the ground-state spectrum. Red dashed line in the theoretical set of curves corresponds to the calculations for the excited-state using FDM, while the dotted blue line corresponds to the calculated data with the multidimensional interpolation approximation. Squares in the experimental set of curves corresponds to the excited-state, while the red dashed line is the spectrum of $[Cu(II)(dmp)_2]^{2+}$ generated electrochemically. Bottom panel: squares are the experimental difference between spectra of $[Cu(dmp)_2]^+$ in the excited and ground states; black solid line is the experimental difference between spectra of $[Cu(II)(dmp)_2]^{2+}$ generated electrochemically and in the ground state; red dashed line is the theoretical difference between spectra of $[Cu(dmp)_2]^+$ in the excited and ground states; solid blue line is the difference between spectra of the excited $[Cu(dmp)_2]^+$ calculated using FDM and the multidimensional interpolation approximation.

Apparently, the shape of the difference spectrum is well reproduced by the calculations in the energy range >8.99 keV. In the experimental spectrum, the first negative sharp peak at 8.985 keV is more intense and shifts, as a result of the slightly higher energy of peak P in the theoretical spectrum of $[Cu(dmp)_2]^+$ in the ground state. It can be due to uncertainties of constructed molecular potentials, but it does not affect the results of geometry optimization because the energy range for the fitting is above 8.99 keV. The best fit values of structural parameters are the following: average $Cu-N_{dmp}$ distance, 2.04 Å; $Cu-N_{CH3CN}$ distance, 2.0 Å; the angle $N_{CH3CN}-Cu-C_2$ axis of dmp, 108°; and the axial rotation of dmp ligands, 16°.

The structural parameters obtained in the present study correlate with those from X-ray diffraction data of a related Cu(II) complex with phenanthroline ligands[51] (average $Cu-N_{dmp}$ distance is 2.04 Å, $Cu-N_{CH3CN}$ distance is 2.05 Å, and the angle between $N_{CH3CN}-Cu$ and the C_2 axis of dmp is 113°). A contraction of the average Cu−N bond length in the excited-state by 0.02 Å from our calculation demonstrated a good agreement with the EXAFS value of 0.04 Å. Nevertheless, our model is significantly different from those obtained using the DFT geometry optimization technique[20,48] where the $Cu-N_{CH3CN}$ distance is 3.05 Å and the rocking distortions are very small. It is well-known that the result of such geometry optimization depends on the starting model that could converge in a geometry corresponding to a local total energy minimum. Therefore, the structure optimized by the DFT calculation may

exist as a transient intermediate during the photochemical reaction, such as the so-called "flattened" MLCT state before it ligates with a solvent molecule. Comparison of XANES spectra of photoexcited molecules in acetonitrile and toluene indicated their strong similarities. Therefore we suggest that rocking distortions could also occur in toluene. The excited-state lifetime difference for $[Cu(I)(dmp)_2]^+$ in these solvents can be explained by the fact that the N atom of acetonitrile has a lone pair electron to facilitate a stronger ligation with the MLCT state, while such a lone pair electron is absent in the C atoms from toluene.

4. Conclusions

Fitting experimental XANES spectra of an exciplex structure of the excited state $[Cu(dmp)_2]^+$ complex has been demonstrated by using a multidimensional interpolation approximation and nonmuffin-tin molecular potentials in theoretically calculated XANES spectra. This combined approach can be used for determination and refinement of three-dimensional structure of photoexcited state of molecules in solution beyond the radial distribution obtained from a conventional EXAFS analysis. The XANES calculations also allow angular dependent structural parameters to be extracted, which is crucial for imaging reaction coordinate of many photochemical reactions. This technique presents broad perspectives in photochemistry and photophysics, and can serve as a basis for structural investigations in ultrafast processes using femtosecond X-ray sources, such as the forthcoming X-ray free electron lasers.

Acknowledgment. This research was supported by the INTAS Grant 06-1000014-6493 and a joint Civilian Research and Development Fund Grant (U.S., # RUC1-2870-RO-07)/ Russian Foundation of Basic Research (Russia, 07-03-91142). A part of this work is supported by the Division of Chemical Sciences, Office of Basic Energy Sciences, U.S. Department of Energy, under contracts DE-AC02-06CH11357 (L.X.C.).

References and Notes

(1) Ruthkosky, M.; Kelly, C. A.; Castellano, F. N.; Meyer, G. J. *Coord. Chem. Rev.* **1998**, *171*, 309.
(2) Wang, X.; Del Guerzo, A.; Schmehl, R. H. *J. Photochem. Photobiol. C* **2004**, *5*, 55.
(3) Mataga, N.; Chosrowjan, H.; Taniguchi, S. *J. Photochem. Photobiol. C* **2005**, *6*, 37.
(4) Waterland, M. R.; Howell, S. L.; Gordon, K. C.; Burrell, A. K. *J. Phys. Chem. A* **2005**, *109*, 8826.
(5) Vauthey, E. *J. Photochem. Photobiol. A* **2006**, *179*, 1.
(6) Garcia, C. G.; de Lima, J. F.; Murakami Iha, N. Y. *Coord. Chem. Rev.* **2000**, *196*, 219.
(7) Gust, D.; Moore, T. A.; Moore, A. L. *Acc. Chem. Res.* **2001**, *3*, 4–40.
(8) Fox, M. A. *Synthetic Applications of Photocatalytic Oxidation and Reduction Reactions of Organic Reactants on Irradiated Semiconductor Surfaces*; Wiley-VCH: New York, 2001; Vol. 1.
(9) Chen, L. X. *Angew. Chem., Int. Ed.* **2004**, *43*, 2886.
(10) Bressler, C.; Chergui, M. *Chem. Rev.* **2004**, *104*, 1781.
(11) Wuilleumier, F. J.; Meyer, M. *J. Phys. B: At., Mol. Opt. Phys.* **2006**, *39*, R425.
(12) Chen, L. X. *Annu. Rev. Phys. Chem.* **2005**, *56*, 221.
(13) Schoenlein, R. W.; Chattopadhyay, S.; Chong, H. H. W.; Glover, T. E.; Heimann, P. A.; Shank, C. V.; Zholents, A. A.; Zolotorev, M. S. *Science* **2000**, *287*, 2237.
(14) Schoenlein, R. W.; Chattopadhyay, S.; Chong, H. H. W.; Glover, T. E.; Heimann, P. A.; Leemans, W. P.; Shank, C. V.; Zholents, A.; Zolotorev, M. *Appl. Phys. B: Laser Opt.* **2000**, *71*, 1.
(15) Tschentscher, T. *Chem. Phys.* **2004**, *299*, 271.
(16) Schneider, J. R. *Nucl. Instrum. Methods Phys. Res., Sect. A* **1997**, *398*, 41.
(17) Feldhaus, J.; Arthur, J.; Hastings, J. B. *J. Phys. B* **2005**, *38*, S799.
(18) Chen, L. X.; Jager, W. J. H.; Jennings, G.; Gosztola, D. J.; Munkholm, A.; Hessler, J. P. *Science* **2001**, *292*, 262.
(19) Chen, L. X.; Jennings, G.; Liu, T.; Gosztola, D. J.; Hessler, J. P.; Scaltrito, D. V.; Meyer, G. J. *J. Am. Chem. Soc.* **2002**, *124*, 10861.
(20) Chen, L. X.; Shaw, G. B.; Novozhilova, I.; Liu, T.; Jennings, G.; Attenkofer, K.; Meyer, G. J.; Coppens, P. *J. Am. Chem. Soc.* **2003**, *125*, 7022.
(21) Saes, M.; Bressler, C.; Abela, R.; Grolimund, D.; Johnson, S. L.; Heimann, P. A.; Chergui, M. *Phys. Rev. Lett.* **2003**, *90*, 047403.
(22) Chen, L. X.; Shaw, G. B.; Liu, T.; Jennings, G.; Attenkofer, K. *Chem. Phys.* **2004**, *299*, 215.
(23) Tomov, I. V.; Rentzepis, P. M. *ChemPhysChem* **2004**, *5*, 27–35.
(24) Lee, T.; Jiang, Y.; Rose-Petruck, C. G.; Benesch, F. *J. Chem. Phys.* **2005**, *122*, 084506.
(25) Khalil, M.; Marcus, M. A.; Smeigh, A. L.; McCusker, J. K.; Chong, H. H. W.; Schoenlein, R. W. *J. Phys. Chem. A* **2006**, *110*, 38.
(26) Gawelda, W.; Pham, V. T.; Benfatto, M.; Zaushitsyn, Y.; Kaiser, M.; Grolimund, D.; Johnson, S. L.; Abela, R.; Hauser, A.; Bressler, C.; Chergui, M *Phys. Rev. Lett.* **2007**, *98*, 057401.
(27) Chen, J.; Zhang, H.; Tomov, I. V.; Ding, X.; Rentzepis, P. M. *Chem. Phys. Lett.* **2007**, *432*, 50.
(28) Chen, L. X.; Zhang, X.; Wasinger, E. C.; Attenkofer, K.; Jennings, G.; Muresan, A. Z.; Lindsey, J. S. *J. Am. Chem. Soc.* **2007**, *129*, 9616.
(29) Larsson, J. *Meas. Sci. Technol.* **2001**, *12*, 1835.
(30) Cole, J. M. *Chem. Soc. Rev.* **2004**, *33*, 501.
(31) Perman, B.; Srajer, V.; Ren, Z.; Teng, T. Y.; Pradervand, C.; Ursby, T.; Bourgeois, D.; Schotte, F.; Wulff, M.; Kort, R.; Hellingwerf, K.; Moffat, K. *Science* **1998**, *279*, 1946.
(32) Smolentsev, G.; Soldatov, A. V. *J. Synchrotron Radiat.* **2006**, *13*, 19.
(33) Benfatto, M.; Della-Longa, S. *J. Synchrotron Radiat.* **2001**, *8*, 1087.
(34) Smolentsev, G.; Soldatov, A. V. *Comput. Mater. Sci.* **2007**, *39*, 569.
(35) Rehr, J. J.; Kozdon, J.; Kas, J.; Krappe, H. J.; Rossner, H. H. *J. Synchrotron Radiat.* **2005**, *12*, 70.
(36) Smolentsev, G.; Soldatov, A. V.; Feiters, M. C. *Phys. Rev. B* **2007**, *75*, 144106.
(37) Smolentsev, G.; Soldatov, A. V.; D'Acapito, F.; Polzonetti, G.; Fratoddi, I. *J. Phys.: Condens. Matter* **2006**, *18*, 759.
(38) Battocchio, C.; D'Acapito, F.; Smolentsev, G.; Soldatov, A. V.; Fratoddi, I.; Contini, G.; Davoli, I.; Polzonetti, G.; Mobilio, S. *Chem. Phys.* **2006**, *325*, 422.
(39) Smolentsev, G.; Feiters, M. C.; Soldatov, A. V. *Nucl. Instrum. Methods Phys. Res., Sect. A* **2007**, *575*, 168.
(40) Hayakawa, K.; Hatada, K.; D'Angelo, P.; Della Longa, S.; Natoli, C. R.; Benfatto, M. *J. Am. Chem. Soc.* **2004**, *126*, 15618.
(41) Sarangi, R.; Benfatto, M.; Hayakawa, K.; Bubacco, L.; Solomon, E. I.; Hodgson, K. O.; Hedman, B. *Inorg. Chem.* **2005**, *44*, 9652.
(42) Benfatto, M.; Della Longa, S.; Hatada, K.; Hayakawa, K.; Gawelda, W.; Bressler, C.; Chergui, M. *J. Phys. Chem. B* **2006**, *110*, 14035.
(43) Pandey, R. K.; Mukamel, S. *J. Phys. Chem. A* **2007**, *111*, 805.
(44) Shaw, G. B.; Grant, C. D.; Castner, E. W.; Meyer, G. J.; Chen, L. X. *J. Am. Chem. Soc.* **2007**, *129*, 2147.
(45) Frisch, M. J.; Trucks, G. W.; Schlegel, H. B.; Scuseria, G. E.; Robb, M. A.; Cheeseman, J. R.; Zakrzewski, V. G.; Montgomery, J. A., Jr.; Stratmann, R. E.; Burant, J. C.; Dapprich, S.; Millam, J. M.; Daniels, A. D.; Kudin, K. N.; Strain, M. C.; Farkas, O.; Tomasi, J.; Barone, V.; Cossi, M.; Cammi, R.; Mennucci, B.; Pomelli, C.; Adamo, C.; Clifford, S.; Ochterski, J.; Petersson, G. A.; Ayala, P. Y.; Cui, Q.; Morokuma, K.; Malick, D. K.; Rabuck, A. D.; Raghavachari, K.; Foresman, J. B.; Cioslowski, J.; Ortiz, J. V.; Stefanov, B. B.; Liu, G.; Liashenko, A.; Piskorz, P.; Komaromi, I.; Gomperts, R.; Martin, R. L.; Fox, D. J.; Keith, T.; Al-Laham, M. A.; Peng, C. Y.; Nanayakkara, A.; Gonzalez, C.; Challacombe, M.; Gill, P. M. W.; Johnson, B. G.; Chen, W.; Wong, M. W.; Andres, J. L.; Head-Gordon, M.; Replogle, E. S.; Pople, J. A. *Gaussian 98*, revision A.9; Gaussian, Inc.: Pittsburgh, PA, 1998.
(46) te Velde, G.; Bickelhaupt, F. M.; van Gisbergen, S. J. A.; Fonseca Guerra, C; Baerends, E. J.; Snijders, J. G.; Ziegler, T. *J. Comput. Chem.* **2001**, *22*, 931.
(47) Zgierski, M. Z. *J. Chem. Phys.* **2003**, *118*, 4045.
(48) Coppens, P.; Novozhilova, I. V. *Int. J. Quant. Chem.* **2005**, *101*, 611.
(49) Miller, M. T.; Gantzel, P. K.; Karpishin, T. B. *Inorg. Chem.* **1998**, *37*, 2285.
(50) Siddique, Z. A.; Yamamoto, Y.; Ohno, T.; Nozaki, K. *Inorg. Chem.* **2003**, *42*, 6366.
(51) Bush, P. M.; Whitehead, J. P.; Pink, C. C.; Gramm, E. C.; Eglin, J. L.; Watton, S. P.; Pence, L. E. *Inorg. Chem.* **2001**, *40*, 1871.
(52) Joly, Y. *Phys. Rev. B* **2001**, *63*, 125120.
(53) Ankudinov, A. L.; Ravel, B.; Rehr, J. J.; Conradson, S. D. *Phys. Rev. B* **1998**, *58*, 7565.
(54) Kovalevsky, A. Yu.; Gembicky, M.; Novozhilova, I. V.; Coppens, P. *Inorg. Chem.* **2003**, *42*, 8794.

JP801410A